The Dynamics of Nucleation in Cahn-Hilliard-Cook Systems

Mahmoud Namazi

Mentor: Dr. Evelyn Sander

Abstract. The Cahn-Hilliard-Cook stochastic partial differential equation describes the process of phase separation in a binary alloy. One common phenomenon that occurs in this model is nucleation where one metal forms droplets in the other. This research considers the droplet distribution in the entire domain, the interior, and the boundary when different boundary conditions are applied. We use various homological tools in order to analyze the Cahn-Hilliard model with Neumann and periodic boundary conditions. Simulations show that, with Neumann boundary conditions, droplets will form more frequently on the boundary of the domain. In contrast, with periodic boundary conditions, simulations show that droplets are form in an evenly distributed manner which scales with the area of the domain.

1. Introduction

The Cahn-Hilliard-Cook stochastic partial differential equation models the concentration of two metals in a binary alloy as a function of space and time. At a high temperature, a mixture of two metals is homogeneous, but after quenching and solidification, the two metals will separate out. The Cahn-Hilliard-Cook serves as a phenomenological model for this process of separation. There are two major known behaviors observed in the Cahn-Hilliard-Cook model, spinodal decomposition (Figure 1), where the two metals form an intertwined snake-like pattern, and nucleation (Figure 2), where one metal forms droplets in the other.

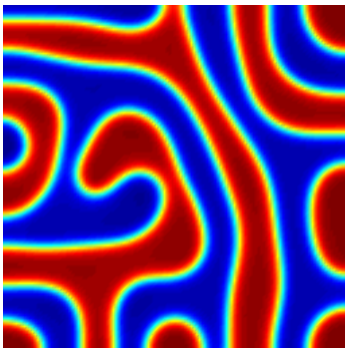

Figure 1. An example of spinodal decomposition.

In this paper, our focus will be on nucleation, which is where one component forms droplets within the other component, as can be seen in Figure 2 where the metal represented by the parts of the domain in blue is forming droplets in the red part of domain which represents the other metal. Similar research has been done on ternary alloys [1]. Our interest is in looking at the effect of periodic and Neumann boundary conditions on droplet formation which can be analyzed using topological data analysis tools.

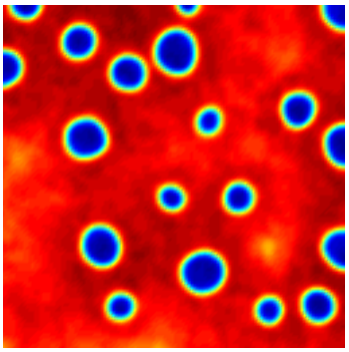

FIGURE 2. An example of nucleation.

2. Preliminaries

The Cahn-Hilliard-Cook stochastic PDE, which was developed by Cahn and Hilliard [2, 3, 4] then extended by Cook [5], models the concentration of two metals in a binary alloy as a function of space and time:

$$u_t = -\Delta(\epsilon^2 \Delta u + f(u)) + \sigma_{noise} \cdot \xi \qquad \text{in} \quad \Omega \quad \text{where} \quad \Delta = \frac{\partial^2 u}{\partial x^2} + \frac{\partial^2 u}{\partial y^2} \quad .$$

The function -f(u) is the derivative of the double-well potential, F, seen in Figure 3. In this case, f(u) = u - u^3 was used. It can be observed that the Cahn-Hilliard-Cook equation is fourth order and non-linear. As stated before, it has spatial and temporal dimensions. Since it does not have a unique solution, boundary conditions are needed, in particular, Neumann and periodic boundary conditions will be discussed. The parameter u describes the difference in the mass concentrations of the two metals in the alloy, $u \in$ [-1, 1]. We interpret values of +1 as being 100% metal A and values of -1 it is 100% metal B. The parameter ϵ is the interaction length, it is a dimensionless quantity which describes the interaction distance at the atomic scale. This is the independent value which we will attempt to relate to the number of droplets formed. It will be shown that changing ϵ is equivalent to rescaling the area of the domain. σ, the amount of noise, perturbs the solution at each time step which drives the solution out of valleys where it takes a deterministic form, namely spinodal decomposition. It is important that this be set correctly as too much noise will obscure the behavior of the equation while too little will cause deterministic behavior, where nucleation is not observed.

One way that droplet formation using this model will be analyzed is with Neumann boundary conditions. On the domain Ω = [0, 1] x [0, 1] $\subseteq \mathbb{R}^2$, let

$$\frac{\partial u}{\partial \nu} = \frac{\partial \Delta u}{\partial \nu} = 0 \quad \text{where } \nu \text{ is the outward normal vector}$$

Another way in which this system will be examined is with periodic boundary conditions where droplets that go over the edge of the domain reappear on the other side. On the domain Ω = [0, 1] x [0, 1] $\subseteq \mathbb{R}^2$, this means

$$u(0, y) = u(1, y) \quad \text{and} \quad u(x, 0) = u(x, 1).$$

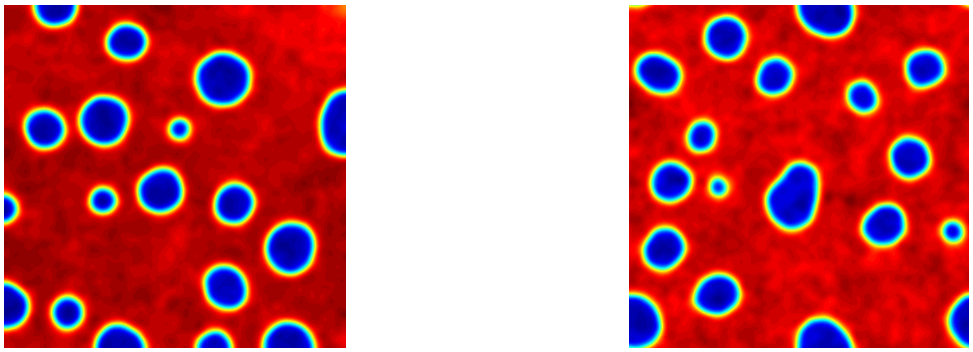

FIGURE 3. The graphic on the left shows a solution to the Cahn-Hilliard-Cook equation with Neumann boundary conditions while the graphic on the right shows a solution to the Cahn-Hilliard-Cook equation with periodic boundary conditions. Notice that with periodic boundary conditions, droplets which go over the edge reappear on the opposite side of the domain, this does not occur with Neumann boundary conditions.

The total mass of the system, M(t) = $\int_\Omega u dx$, is conserved, to show this let

$$\frac{d}{dt}M(t) = \frac{d}{dt}\int_\Omega u dx = \int_\Omega u_t dx = \int_\Omega -\Delta(\epsilon^2\Delta u + f(u))dx$$

Next, using the divergence theorem,

$$\frac{d}{dt}M(t) = \int_{\partial\Omega} \nabla\left(\epsilon^2\Delta u + f(u)\right)\cdot\nu\, ds \; - \int_\Omega \nabla 1 dx$$

The gradient of the entire equation on the boundary, with respect to the direction of the normal vector, is zero. The gradient of 1 is zero as well. Therefore

$$\frac{d}{dt}M(t) = 0$$

μ being the average mass, let

$$\mu \;=\; \frac{1}{\Omega}\cdot\int_\Omega u dx \quad \text{with} \quad |\Omega| \;=\; \int_\Omega 1 dx.$$

This means that only the local concentration difference will change, while the overall concentration difference in the alloy will stay constant.

The Van Der Waals free energy functional can be stated as follows:

$$E_\epsilon[u] \;=\; \int_\Omega \left(\frac{\epsilon^2}{2}|\nabla u|^2 \;+\; F(u)\right)$$

The energy gives an idea of how the function behaves since dE/dt $\leq$ 0. This can be proven analytically:

$$\begin{aligned}\frac{dE}{dt} \;&=\; \frac{d}{dt}\int_\Omega \left(\frac{\epsilon^2}{2}|\nabla u|^2 \;+\; F(u)\right)\\ &=\; \int_\Omega \left(\epsilon^2\nabla u\cdot\nabla u_t + \; F'(u)u_t\right)\end{aligned}$$

Using the divergence theorem on the first term and the fact that F'(u) = -f(u) on the second, we get:

$$\frac{dE}{dt} = \int_{\partial\Omega} \epsilon^2 u_t \nabla u \cdot \nu \, ds - \int_\Omega \left(\epsilon^2 u_t \Delta u\right) dx - \int_\Omega \left(f(u) u_t\right) dx$$

With Neumann boundary conditions, the gradient in the direction of the normal vector, n, is zero. Therefore this integral goes to zero, so:

$$\frac{dE}{dt} = -\int_\Omega \left(\left(\epsilon^2 \Delta u + f(u)\right) u_t\right) dx$$

Next, substituting the Cahn-Hilliard equation for u_t:

$$\frac{dE}{dt} = \int_\Omega \left(\left(\epsilon^2 \Delta u + f(u)\right) \Delta(\epsilon^2 \Delta u + f(u)\right) dx$$

Next, the divergence theorem is used once more:

$$\frac{dE}{dt} = \int_{\partial\Omega} \left(\epsilon^2 \Delta u + f(u)\right) \nabla \left(\epsilon^2 \Delta u + f(u)\right) \cdot \nu \, ds - \int_\Omega \left(\nabla \left(\epsilon^2 \Delta u + f(u)\right) \nabla \left(\epsilon^2 \Delta u + f(u)\right)\right) dx$$

Further developing the second term in the first integral:

$$\int_{\partial\Omega} \left(\epsilon^2 \Delta u + f(u)\right) \left(\epsilon^2 \nabla(\Delta u) + \nabla u - 3u(u_x + u_y)\right) \cdot \nu \, ds$$

Due to Neumann boundary conditions, $\Delta u \cdot \nu$ goes to zero, as does $-3u(u_x + u_y) \cdot \nu = -3u(\nabla u) \cdot \nu$. Therefore, this entire integral goes to zero, leaving:

$$\frac{dE}{dt} = -\int_\Omega \left(|\nabla \left(\epsilon^2 u_t \Delta u\right)|^2\right) dx \leq 0$$

Therefore, it can be seen that first term in the energy, $\frac{\epsilon^2}{2}|\nabla u|^2$, minimizes gradients such that there is a sharp interface between any droplets and the other metal. The second term, $F(u)$, which is the double well potential (Figure 4), minimizes non-pure components. The lowest energies occur at +1 and -1 in the plot, signifying that the global energy minimum is present in pure domains. The minimization of these values, combined with the small perturbations caused by the noise, lead to nucleation since these perturbations will cause many gradients to form throughout the domain which the function will seek to minimize while at the same time droplets of metal will form due to the preference for pure components.

The fact that minimization of gradients occurs is critical to this research. It is hypothesized that due to this, when Neumann boundary conditions are present, droplets will form more frequently on the boundary of the domain in order to minimize the gradient between the two metals. With periodic boundary conditions, since droplets wrap around the edges, a more even distribution of droplets throughout the domain is expected since no energy advantage exists at the edge of the domain.

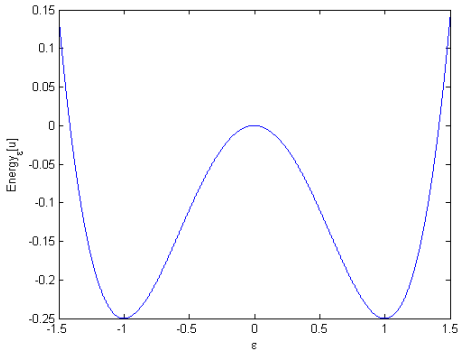

FIGURE 4. This double-well potential gives the energy as a function of the value of the domain, notice that the pure domains at +1 and -1 are global minima.

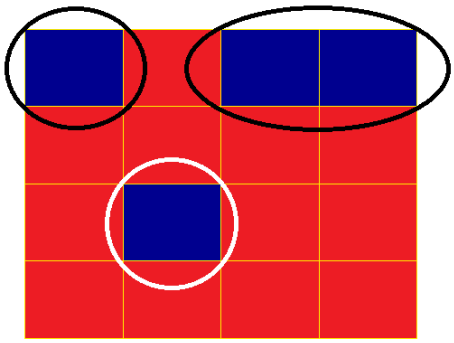

FIGURE 5. An extremely simplified solution, the only interior droplet is circled in white and the boundary droplets are circled in black.

Besides the total number of droplets, one can talk about boundary and interior droplets (Figure 5). Boundary droplets are defined as those droplets which touch the boundary of the domain and interior droplets are defined as those that do not. In order to differentiate between an interior and boundary droplet, which is required in order to analyze the effect of the periodic and Neumann boundary conditions on droplet formation, some algebraic topology is needed. The Euler characteristic [6]

$$\chi := \text{Vertices} - \text{Edges} + \text{Faces}$$

is a topological property that can be used to describe the topology of a structure and gives information about the geometric properties of a space. It is a topological invariant, meaning that two solutions with the same number of droplets (of the same type, interior and boundary) will give the same the Euler characteristic. In addition to Betti numbers, it provides a computationally-feasible way to count droplets. In a cube, there are 8 vertices, 12 edges, and 6 faces so therefore $\chi = 8 - 12 + 6 = 2$. In the following example (Figure 6), a hexagonal prism, there are 12 vertices, 18 edges, and 8 faces so therefore $\chi = 12 - 18 + 20 = 2$. In fact, for all convex polyhedron $\chi = 2$ [6]. It is not possible to know all of the Betti numbers, and therefore all of the information about the interior/boundary droplets, without the Euler characteristic.

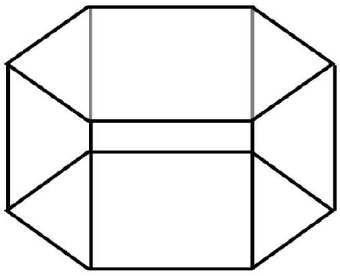

FIGURE 6. A hexagonal prism.

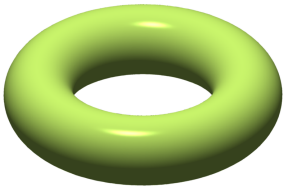

FIGURE 7. A torus.

Betti numbers are another topological invariant descriptor of topological spaces, they tell us how the space is connected [7]. Each Betti number gives a piece of information about the space of interest: β_0 represents the number of connected components, β_1 represents the number of tunnels or circular holes, and β_2 represents the number of cavities or voids. For Figure 5, from the perspective of the blue component, $\beta_0 = 3$ since there are three distinct blue, connected components, $\beta_1 = 1$ since only the component in the center is a circle (the ones at the edge cannot be holes), and $\beta_2 = 0$ since it is 2-dimensional, and therefore there is no cavity. For the torus above (Figure 7), $\beta_0 = 1$, since it is one connected piece, $\beta_1 = 2$, because there are two circular holes, one is found by following the loop in the center of the torus and the other is found by going around side, and $\beta_2 = 1$, since the inside is an empty cavity.

The following relationship exists between the Euler characteristic and the Betti numbers:

$$V - E + F = \beta_0 - \beta_1 + \beta_2.$$

This relationship is important as it allows the number of boundary and interior droplets to be found computationally. Although it is possible to find the total number of droplets without the relationship between the Euler characteristic and the Betti numbers, it is impossible to differentiate between the interior and boundary droplets without them. In order to find the interior and boundary droplets in Figure 4, first we count the number of vertices, edges, and faces in regards to the red component since we would like to find the number of tunnels. In this case, the number of vertices is 22 (we do not count the two shared vertices between the upper right droplet twice), the number of edges is 34, and the number of faces is 12. This gives an the Euler characteristic of 0 and we know that β_0 for this component is 1 since it is all one connected piece. β_2 is 0 since the presence of droplets in the domain means that no cavity can exists. With the information of the Euler characteristic and the other two Betti numbers, we can solve for β_1 which we will find to be 1, meaning that there is one hole in the red domain meaning that there is one interior droplet, which can be verified visually. Subtracting the number of known interior droplets from the total number of droplets will give the number of boundary droplets which is 2.

The predicted relationship between ϵ and the droplet count is that as ϵ increases, which is analogous to making the domain smaller, a smaller droplet count will be seen that is scaled to a smaller domain. To show this, we consider the Cahn-Hilliard-Cook equation without noise (named the Cahn-Hilliard equation):

$$\frac{\partial u}{\partial t} = -\Delta(\epsilon^2 \Delta u + f(u)) \qquad \text{where} \quad 0 < x < 1 \ \ \& \ \ 0 < y < 1$$

We then define new, scaled time and space parameters:

$$\begin{cases} \tilde{t} = \gamma^2 t \\ \tilde{x} = \gamma x \\ \tilde{y} = \gamma y \end{cases}$$

By rescaling the parameters, the bounds and Laplacian must also be rescaled. Define:

$$\tilde{\Delta} = \frac{\partial^2 u}{\partial \tilde{x}^2} + \frac{\partial^2 u}{\partial \tilde{y}^2} \quad \text{and} \quad 0 < \tilde{x} < \gamma \ \ \& \ \ 0 < \tilde{y} < \gamma$$

Using the chain rule, then the above facts we find we find:

$$\frac{\partial u}{\partial t} = \frac{\partial}{\partial t}\frac{\partial \tilde{t}}{\partial t} \qquad \text{and} \qquad \frac{\partial \tilde{t}}{\partial t} = \frac{\partial}{\partial t}(\gamma^2 t) = \gamma^2$$

Therefore:

$$\frac{\partial u}{\partial t} = \gamma^2 \frac{\partial u}{\partial \tilde{t}}$$

This corresponds to the left-hand side of the Cahn-Hilliard equation. This tells us that the change in the concentration of the alloy as a function of time can be rescaled in time by a factor γ^2. Similarly, space can be rescaled:

$$\frac{\partial u}{\partial x} = \frac{\partial u}{\partial \tilde{x}}\frac{\partial \tilde{x}}{\partial x} = \gamma \frac{\partial u}{\partial \tilde{x}}$$

We see the same relationship here as we saw with time, except in this case the scaling factor is not squared. This same argument works for space in the y direction. Next, the Laplacian is rescaled:

$$\frac{\partial^2 u}{\partial x^2} = (\gamma \frac{\partial u}{\partial \tilde{x}})(\gamma \frac{\partial u}{\partial \tilde{x}}) = \gamma^2 \frac{\partial^2 u}{\partial \tilde{x}^2}$$

A similar argument is made for space in y dimension. Putting these together:

$$\Delta u = \frac{\partial^2 u}{\partial x^2} + \frac{\partial^2 u}{\partial y^2} = \gamma^2 \frac{\partial^2 u}{\partial \tilde{x}^2} + \gamma^2 \frac{\partial^2 u}{\partial \tilde{y}^2} = \gamma^2 \tilde{\Delta} u$$

Putting together these rescaled parameters in the Cahn-Hilliard equation:

$$\gamma^2 \frac{\partial u}{\partial \tilde{t}} = -\gamma^2 \tilde{\Delta}(\epsilon_n{}^2 \gamma^2 \tilde{\Delta} u + f(u)) \qquad \text{on} \quad (0,\gamma)^2$$

Dividing both sides by γ^2 and setting $\gamma = \epsilon_0/\epsilon_n$, we get:

$$\frac{\partial u}{\partial \tilde{t}} = -\tilde{\Delta}(\epsilon_0{}^2 \tilde{\Delta} u + f(u)) \qquad \text{on} \quad (0, \frac{\epsilon_0}{\epsilon_n})^2$$

This implies that a change from a fixed ϵ, ϵ_0, to a new value, ϵ_n, can be viewed instead as a rescaling of the domain from $(0,1)^2$ to $(0,\frac{\epsilon_0}{\epsilon_n})^2$, with ϵ_0 remaining fixed, since the number of droplets will change, but not the size of the droplets. However, due to the energy of being close to the boundary of the domain when the equation is evaluated with Neumann boundary conditions, it is expected that up to some width, d, the boundary will dominate the interior in terms of number of droplets and so this width must be taken into account. The prediction that there will be an unevenly distributed number of droplets within the width of the boundary versus the interior of the domain means that the total number of droplets and the number of droplets in the interior cannot be described by a single equation and that both equations must take into account this width, d. In order to get a sense of how the width is used to separate the interior and boundary, refer to Figure 8. Based on this, if there are a known number of interior droplets, i_0, in the interior region $(d,1-d)^2$ for ϵ_0, the number of interior droplets for ϵ_n, i_n, is expected to be the same as the number in the interior region $(d,\frac{\epsilon_0}{\epsilon_n}-d)^2$ for ϵ_0. Therefore, in terms of relative size, we are scaling from $(1-2d)^2$ to $(\frac{\epsilon_0}{\epsilon_n}-2d)^2$, where 2d accounts for the width on each side of the domain, and so

$$i_n = i_0 \cdot \frac{(\frac{\epsilon_0}{\epsilon_n}-2d)^2}{(1-2d)^2}$$

This equation can be used to formulate another equation to predict the number of total droplets as a function of ϵ. This equation

$$t_n = t_0 \cdot \frac{(\frac{\epsilon_0}{\epsilon_n}+2d)^2}{(1+2d)^2}$$

is predicted to give the number of total droplets as a result of the change in ϵ. Here, the 2d corresponds to the adding of an edge on two sides of the domain, to account for "full" boundary droplets via reflection.

In terms of periodic boundary conditions, since there is no energy advantage at any particular place, it is expected that the number of droplets scale linearly with the area. So in this case

$$t_n = t_0 \cdot (\frac{\epsilon_0}{\epsilon_n})^2$$

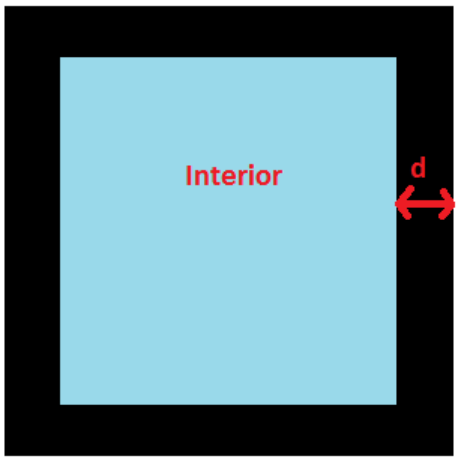

FIGURE 8. A diagram showing how the interior and boundary are defined on the unit square where d is the width of the boundary.

3. Methods

First, the numerical methods will be described. The model was run with Neumann boundary conditions and periodic boundary conditions on the domain $\Omega = (0, 1)^2$. The spectral method [8] was used to solve the equation with the Discrete Cosine Transform used when solving it with Neumann boundary conditions and the Fast Fourier Transform used when solving the equation with periodic boundary conditions. The time step was varied across each of the ϵ values in order to get the finest sampling as possible, this is described in more detail later on. The solution was approximated by 128^2 Fourier modes, the number of coefficients used to approximate the solution in the frequency domain where calculations in the spectral method are carried out. The model was adapted to periodic boundary conditions from a model originally written with Neumann boundary conditions by Sander, Stephens, and Wanner.

In order to find the total number of droplets, or β_0, a breadth first search algorithm [9] was used. The algorithm, in this context, first creates a new matrix where each point below a certain numerical value becomes one of two binary values, and values above or equivalent to this threshold become the other value. In this way, the different metal components can be analyzed. Next, the first value in the matrix associated with the metal component we are interested in is found. This becomes the initial point. A counter is started at 1 and the initial point in the binary matrix is changed to a 1. Next, each adjacent point is checked, for example if (1,1) was the first point found, then points (1,2), (2,2), and (2,1) are checked. If these are also the metal component being looked at, then these points are also marked as 1 and we progress to the last checked point in order to check this new point's neighbors. Once each of the adjacent points has been checked, we backtrack to the most recent marked points whose neighbors were not checked and check the points adjacent to those as well. This process repeats until none of the adjacent points are found to be the same metal component. The process is then started from the beginning by choosing the next point in the matrix of the metal component that is being looked at (who's value will be one of the binary values chosen at the beginning, in this way we never go back to a point already marked). The counter is now increased by 1 when marking these new points. Once no new points can be found, the counter will give the total number of nodal components. In this way, β_0 is found for each metal in the binary alloy. In the periodic case, a modulus function was introduced where if the modulus of the current point in the x or y direction and the maximum size of the matrix in that direction was found to be 0, then the current point would be changed to the point exactly across from it on the matrix. In this way, boundary droplets would not be split up in a periodic analysis of the periodic simulation.

In terms of numerical speed, breadth first search takes $O(b^d)$ time, where b is the branching factor and d is the depth of the solution, which is dependent on the size of the particular droplet. Another algorithm that could be used is a depth first search where instead of first marking all adjacent points, one adjacent point is followed by the next and every adjacent is not marked. Then, once newer points fail to be found, backtracking is done and new paths are found.

In order to find the Euler characteristic, first the solution is taken.

FIGURE 9. A sample solution to the Cahn-Hilliard equation.

In a real simulation, the domain is made up of a very fine grid so that the solution looks continuous. However, in this example, since we would like to demonstrate how the Euler characteristic is computed, we will digitize our solution into a 4 x 4 matrix. A simple demonstration will easily carry over into the actual simulation where a 256 x 256 matrix is used.

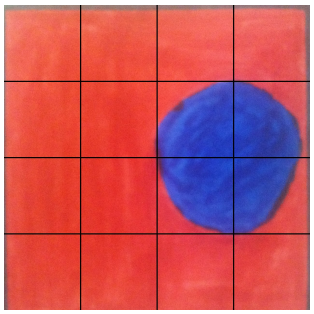

FIGURE 10. The digitalization of the solution.

Next, a new matrix is created with a single extra column and row on each side. Values from the solution matrix will be converted into one of two binary numbers, representing the two different metal components (the component forming the droplets is set to one, for addition purposes), and placed in the center.

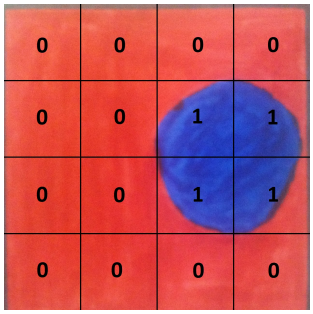

$$\begin{matrix} 0 & 0 & 0 & 0 & 0 & 0 \\ 0 & 0 & 0 & 0 & 0 & 0 \\ 0 & 0 & 0 & 1 & 1 & 1 \\ 0 & 0 & 0 & 1 & 1 & 1 \\ 0 & 0 & 0 & 0 & 0 & 0 \\ 0 & 0 & 0 & 0 & 0 & 0 \end{matrix}$$

FIGURE 11. First a threshold is applied to the matrix, here faces that correspond to the metal that is forming the droplet are set to 1 and the other metal to 0. Next, this matrix is placed in the center of a new matrix with one additional row and one additional column on each side.

Each value of the solution next to the new row/column will be copied unto the adjoining new row/column, this is needed to take care of having the correct number of edges and vertices around

the corners since each matrix value corresponds to a face. Simply by looking at the original, 4x4 matrix and adding up the number of ones, we find that the number of faces is 4.

Next, the vertices are found by taking the inclusive OR of four smaller matrices corresponding to each corner of the larger matrix with an edge on the one vertical side and one horizontal side excluded. This method prevents the counting of any vertex twice. This process can be seen in Figure 12.

$$\begin{matrix} 0 & 0 & 0 & 0 & 0 \\ 0 & 0 & 0 & 0 & 0 \\ 0 & 0 & 0 & 1 & 1 \\ 0 & 0 & 0 & 1 & 1 \\ 0 & 0 & 0 & 0 & 0 \end{matrix} \quad \begin{matrix} 0 & 0 & 0 & 0 & 0 \\ 0 & 0 & 0 & 1 & 1 \\ 0 & 0 & 0 & 1 & 1 \\ 0 & 0 & 0 & 0 & 0 \\ 0 & 0 & 0 & 0 & 0 \end{matrix} \quad \begin{matrix} 0 & 0 & 0 & 0 & 0 \\ 0 & 0 & 0 & 0 & 0 \\ 0 & 0 & 1 & 1 & 1 \\ 0 & 0 & 1 & 1 & 1 \\ 0 & 0 & 0 & 0 & 0 \end{matrix} \quad \begin{matrix} 0 & 0 & 0 & 0 & 0 \\ 0 & 0 & 1 & 1 & 1 \\ 0 & 0 & 1 & 1 & 1 \\ 0 & 0 & 0 & 0 & 0 \\ 0 & 0 & 0 & 0 & 0 \end{matrix}$$

$$\begin{matrix} 0 & 0 & 0 & 0 & 0 \\ 0 & 0 & 1 & 1 & 1 \\ 0 & 0 & 1 & 1 & 1 \\ 0 & 0 & 1 & 1 & 1 \\ 0 & 0 & 0 & 0 & 0 \end{matrix}$$

FIGURE 12. The top four matrices correspond to a 5x5 matrix taken from each corner of the new 6x6 matrix. The bottom matrix is the result of taking the logical OR of the top four matrices.

By adding up the ones in the final matrix, we find the number of vertices to be 9.

Next, in order to find the number of edges, a similar method is used. Only the center columns and rows are considered because the number of faces (the number of ones placed in the center by the solution matrix captures the number of faces) is equivalent to the edges shared by each face. The reflections from the center to the new columns on the left and right, and the new rows on the top and bottom, will be covering for the unshared edges by droplets on the edge of the domain. By taking the sum of the inclusive OR of a matrix compromised of the top edge and the center and a matrix compromised of the bottom edge and the center, the number of horizontal edges can be found. This process can be seen in Figure 13.

$$\begin{matrix} 0 & 0 & 0 & 0 \\ 0 & 0 & 0 & 0 \\ 0 & 0 & 1 & 1 \\ 0 & 0 & 1 & 1 \\ 0 & 0 & 0 & 0 \end{matrix} \qquad \begin{matrix} 0 & 0 & 0 & 0 \\ 0 & 0 & 1 & 1 \\ 0 & 0 & 1 & 1 \\ 0 & 0 & 0 & 0 \\ 0 & 0 & 0 & 0 \end{matrix}$$

$$\begin{matrix} 0 & 0 & 0 & 0 \\ 0 & 0 & 1 & 1 \\ 0 & 0 & 1 & 1 \\ 0 & 0 & 1 & 1 \\ 0 & 0 & 0 & 0 \end{matrix}$$

FIGURE 13. The top two matrices correspond to a 5x4 matrix taken from the top-center and the top-bottom of the 6x6 matrix. The bottom matrix is the result of taking the logical OR of the top two matrices. This bottom matrix captures the number of horizontal edges.

Using this method, we find that the number of horizontal edges is 6 by adding together the ones in the final matrix. This is similarly done for the vertical edges, except this time the matrices considered are the center with the new left edge and the center with the new right edge. Doing this, we would find the number of vertical edges to be 6. By adding together the horizontal and vertical edges, we find the total number of edges to be 12.

Using the above described methods which reflect the actual algorithm, we can find the Euler characteristic:

$$\chi := \text{Vertices} - \text{Edges} + \text{Faces} = 9 - 12 + 4 = 1$$

Using β_0 and the Euler characteristic for each nodal component, β_1 for each nodal component can be computed.

A first set of runs was used in order to find the approximate time horizon, or the time at which the total number of droplets peaks. The average of these runs gives a smooth curve which has a maximum that can be computationally found. The time at which this maximum occurs is the time horizon. This can be seen in the plot below of several Betti curves (Figure 14), which is simply a plot of the decomposition of the droplets over time.

Next, a new set of runs was conducted where the end time was set to 20% above the previously found time horizon (to leave room for error). This was conducted for each ϵ value and a unique time step for each was chosen in order to capture the time horizon, but at the same time to get as small of a time step as possible. The new set of runs was then averaged across each ϵ value and the total number of droplets was extracted from the time horizon (based on the maximum number of droplets of this new set of runs, not on the previous set). In order to compute the number of interior droplets, at each time step, the solution was analyzed in the same way the Neumann boundary conditions case was analyzed - by assuming that droplets at the edge do not wrap around the boundary. The average number of interior droplets was extracted from the time horizon of the total number of droplets, which does not necessarily correspond to its own time horizon. It is important to extract droplet totals from the same time step. The width was then calculated, using the interior droplet equation and the two largest ϵ, then used to predict the number of droplets at the other ϵ values. These results are shown below, they were found with 500 runs of the model for each ϵ value.

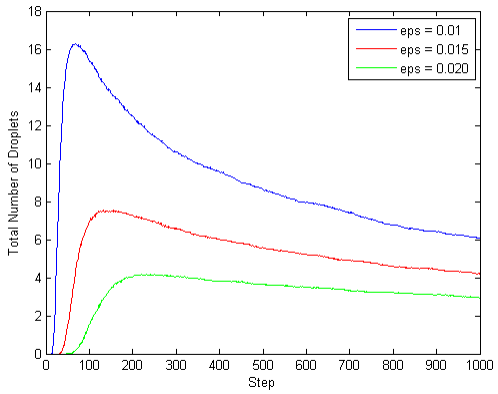

FIGURE 14. Several Betti curves over different ϵ values.

4. Results

The periodic boundary condition solution was analyzed as if it were Neumann, i.e. a distinction was made between interior and boundary droplets. This analysis was important as it allows us to observe the change in the interior of the domain with periodic boundary conditions. Results for a different number of ϵ values were found with periodic boundary conditions versus Neumann boundary conditions because with Neumann boundary conditions, at the ϵ values of 0.025 and 0.020, the number of droplets was so few that it caused a large amount of error in the calculations for the higher ϵ values. The error propagates due to the fact that the width of the boundary is found using the droplet count of the two highest ϵ values.

Below are the numerical results for the interior and total droplets with each type of boundary conditions:

ϵ	Actual Interior	Predicted Interior	Error
0.015	3.82	3.816	0.00%
0.010	10.006	10.006	0.00%
0.005	46.730	46.138	1.27%
0.004	75.012	74.084	1.24%
0.003	136.002	135.294	0.52%

TABLE 1. Neumann boundary conditions, interior droplet predictions and error, d = 0.204

ϵ	Actual Total	Predicted Total	Error
0.015	9.192	9.192	0.00%
0.010	18.224	18.515	1.60%
0.005	63.444	65.871	3.83%
0.004	95.472	100.455	5.22%
0.003	163.210	174.250	6.76%

TABLE 2. Neumann boundary conditions, total droplet predictions and error, d = 0.204

ϵ	Actual Total	Predicted Total	Error
0.025	3.978	3.978	0.00%
0.020	5.782	5.782	0.00%
0.015	9.538	9.536	0.02%
0.010	19.892	19.847	0.23%
0.005	73.752	73.203	0.74%
0.004	113.424	112.492	0.82%
0.003	194.590	196.664	1.07%

TABLE 3. Periodic boundary conditions, total droplet predictions (Neumann analysis) and error, d = 0.107

ϵ	Actual Interior	Predicted Interior	Error
0.025	1.724	1.724	0.00%
0.020	2.920	2.998	2.69%
0.015	5.790	5.901	1.93%
0.010	14.354	14.628	1.91%
0.005	63.084	64.176	1.73%
0.004	100.574	102.094	1.51%
0.003	178.084	184.762	3.75%

TABLE 4. Periodic boundary conditions, interior droplet predictions and error, d = 0.107

ϵ	Actual Interior	Predicted Interior	Error
0.025	2.752	2.752	0.00%
0.020	4.250	4.300	1.18%
0.015	7.596	7.644	0.64%
0.010	17.148	17.200	0.30%
0.005	68.818	68.800	0.03%
0.004	107.776	107.500	0.26%
0.003	187.808	191.111	1.76%

TABLE 5. Periodic boundary conditions, total droplet predictions and error

Beginning with Table 1, we observe that the number of total droplets scaled well when the width was fitted to the two largest ϵ values. However, in Table 2, using the same width, it can be observed that the error magnifies as ϵ gets smaller. As the domain grows linearly in size, the effects of the boundary seem to decrease (which can be observed by the fact that the actual number of interior droplets overshoots the predicted number). This makes sense - on a larger domain it is less likely that a droplet forming in the center will move to the edge, due to the fact that the edge is farther away and simply put, the pull on the droplets towards the edge decreases.

Next, looking at the simulations with periodic conditions, it is first important to note that, as mentioned previously, the analysis is done in two ways. First, we analyze the droplets as if the simulation were conducted with Neumann boundary conditions, that is, two droplets directly across from each other on the opposite edge will be analyzed as two separate droplets. Through this lens, looking at Table 3, it can be seen that the errors for the predicted number of total droplets are

very low. As expected, this is due to the fact that the droplets scale linearly with the size of the domain with periodic boundary conditions. The width in this case is necessary to account for the droplets that we have now identified as boundary droplets. But regardless, it is seen that the total droplets scale with the size of the domain and a fixed width. Looking at Table 4, a similar effect is noticed. Taking out the boundary droplets by subtracting the fixed width, we observe a linear scaling of the interior droplets with the size of the domain.

Finally, in Table 5, the analysis is done in the periodic sense - that is, droplets are analyzed in the same manner which they formed. Droplets that are adjacent across the domain and formed as one droplet going over the edge are considered a single droplet. In this case, with a prediction equation which simply scales the prediction by the change in ϵ, we observe again very low errors. This tells us again that the number of total droplets scaled linearly with the size of the domain.

The errors throughout seemed higher than expected; especially when compared to the paper involving the Cahn-Morral system [1], although it is a multi-component system rather than a binary one. The error was particularly large in Table 2. Possible reasons for the high error include calculating the width based on ϵ values which were too high (as in produced too few droplets thereby skewing the width calculation) and running too few simulation runs.

5. Conclusion

This work has been about analyzing nucleation in the Cahn-Hilliard-Cook equation with Neumann and periodic boundary conditions. As described in the results, we found that with periodic boundary conditions the number of droplets scaled linearly with area, both in terms of the interior and the domain as a whole. In contrast, with Neumann boundary conditions, the results showed that the energy advantage at the boundary of the domain had considerable effect on droplet formation, although this affect diminished with the growing size of the domain. The hypothesis, given by the Van Der Waals free energy functional, proved to be true. With periodic boundary conditions, since the energy benefit for droplets at the boundary of the domain does not exist, droplets distribute evenly throughout the domain. No new long-range effects were found, however, the research showed that it is better to use full droplets with periodic boundary conditions and boundary/interior droplets with Neumann boundary conditions. Future avenues of exploration include conducting a bifurcation analysis and looking at droplet formation in terms of the mass, μ.

6. Acknowledgements

I would like to thank my mentors Dr. Evelyn Sander, Dr. Thomas Wanner, and Tom Stephens along with my REU collaborative partner, Kalea Sebesta. This project was partially supported by NSF grant DMS-0639300.

References

[1] J.P. Desi, H. Edrees, J. Price, E. Sander and T. Wanner, *The Dynamics of Nucleation in Stochastic Cahn-Morral systems*, SIAM Journal on Applied Dynamical Systems, 10 (2011), pp. 707-743.
[2] J. W. Cahn and J. E. Hilliard, *Free energy of a nonuniform system I. Interfacial free energy*, J. Chem. Phys., 28 (1958), pp. 258-267.
[3] J. W. Cahn, *Free energy of a nonuniform system II. Thermodynamic basis*, J. Chem. Phys., 30 (1959), pp. 1121-1124.
[4] J. W. Cahn and J. E. Hilliard, *Free energy of a nonuniform system III. Nucleation in a two-component incompressible fluid*, J. Chem. Phys., 31 (1959), pp. 688-699.
[5] H. Cook, *Brownian motion in spinodal decomposition*, Acta-Metallurgia, 18 (1970), pp. 297-306.
[6] Richeson, David S. *Euler's Gem: The Polyhedron Formula and the Birth of Topology.* Princeton, NJ: Princeton UP, 2008.
[7] Henle, Michael. *A Combinatorial Introduction to Topology.* San Francisco: W.H. Freeman, 1979.

[8] Sander, Evelyn, and Wanner, Thomas. *Nonlinear Analysis and Computation for Partial Differential Equations.* Manuscript.
[9] Cormen, Thomas H. *Introduction to Algorithms.* Cambridge, Mass: MIT Press, 2009.